*Journal of Sound and Vibration* (2002) **252**(5), 919–933
doi:10.1006/jsvi.2001.3873, available online at http://www.idealibrary.com on IDEAL®

# INVESTIGATION ON THE DYNAMIC PERFORMANCE OF THE TRIPOD-BALL SLIDING JOINT WITH CLEARANCE IN A CRANK–SLIDER MECHANISM. PART 1. THEORETICAL AND EXPERIMENTAL RESULTS

X. Jia, D. Jin, L. Ji and J. Zhang

*Room* 3307, *Department of Precision Instruments and Mechanics*, *Tsinghua University*, *Beijing* 100084, *People's Republic of China. E-mail*: *jiaxh@pim.tsinghua.edu.cn*

(*Received* 27 *January* 2000, *and in final form* 4 *July* 2001)

Clearance is inevitable in the kinematic joints of mechanisms. In this paper, the dynamic behavior of a crank–slider mechanism with clearance in its tripod-ball sliding joint is investigated theoretically and experimentally. The mathematical model of this new-type of joint is established, and the new concepts of basal system and active system are put forward. Based on the mode-change criterion established in this paper, the consistent equations of motion in full-scale are derived by using Kane method. The experimental rig was set up to measure the effects of the clearance on the dynamic response. The dynamic responses including additional motion, input torque and acceleration have been obtained, and the effects of the clearance size and driving speed have also been investigated by both analytical and experimental means. Corresponding experimental studies verify the theoretical results satisfactorily. 

## 1. INTRODUCTION

Small clearances in the kinematic joints of mechanisms are necessary for assembly and mobility. However, when clearance size is not suitable, impact will occur due to impulsive acceleration. The occurrence causes a large amplification of machine dynamic force which in turn not only creates increased vibration and noise, but also reduces system reliability, stability, life and precision.

In the past few years, a number of papers have been published in which the effects of clearance on the dynamic behavior of planar or spatial mechanisms were reported. Different kinds of kinematic joints such as revolute joint [1], prismatic joint [2], cylindrical joint [3] and spherical joint [4] with clearance were analyzed with different models [5–9]. However, the tripod-ball sliding joint (TBS joint), as a new type of sliding joint, has different dynamic characteristics under the effect of clearance. The study on its dynamic behavior has not been reported.

In this paper, considering a crank–slider as the mechanism being investigated, the dynamic performance including additional motion, driving torque, reacting forces in joints and contact state of the TBS joint with clearance have been studied analytically and experimentally. The effects of clearance size and driving speed have also been investigated by these two means.

Besides, the basal system and active system are defined to obtain a set of consistent equations of motion for both free-flight and following mode, rather than two different sets of

0022-460X/02/$35.00 

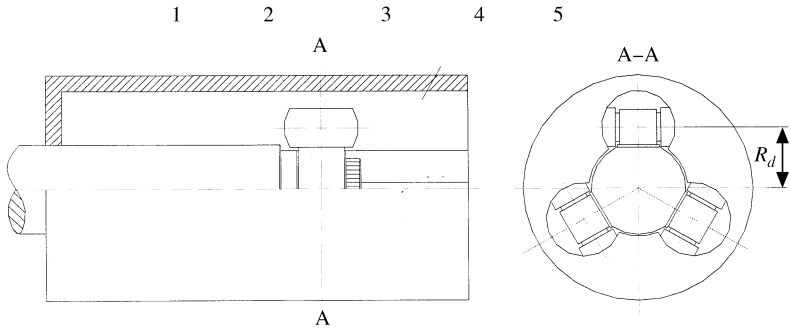


Figure 1. The tripod-ball sliding joint.

equations in other publications. The agreement of numerical and experimental results shows that the analytical procedure presented in this paper is very effective.

## 2. THE TRIPOD-BALL SLIDING JOINT

The TBS joint is shown diagrammatically in Figure 1. Shaft 1 is splined with tripod base 2, which has three pins on the circle of radius $R_d$ equi-spaced in the plane A–A. Ball-rollers 3 are connected with pins through bearings 5, and in the guide sleeve 4 there are three inner cylindrical grooves which match with the three ball-rollers. Through rolling contact between ball-roller and cylindrical groove, the shaft 1 and the guide sleeve 4 can move relatively. Compared with other prismatic joints, the main advantage of the TBS joint is that the friction coefficient is as small as 0·003. Owing to its high transmission efficiency, long life and low wear, it has been widely adopted in many mechanisms, for instance, in the transmission system of high-speed locomotive.

## 3. EQUATIONS OF MOTION

The special system considered here is a crank-slider mechanism with clearance in its tripod-ball sliding joint. As shown in Figure 2, $B_i$ ($i = 0$–4) stands for base, crank, link, slider, groove, respectively, and $O_i$ ($i = 1$–4) is the joint between $B_i$ and $B_{i-1}$, and $C_i$ ($i = 1$–3) is the mass center of $B_i$. Some parameters for this mechanism are shown in Appendix B. In order to investigate the effects of clearances on the motion of the mechanism, the following assumptions are employed. (1) All components are rigid. (2) There are no clearances in other joints except in the TBS joint. (3) The driving speed is constant. (4) The friction in joints is not considered. (5) The rotating motion about $y$-axis of the mechanism is neglected.

The discontinuous contact model is used to describe the dynamics of the system, which contains two distinct modes of motion of the ball-roller in cylindrical groove. One is the free-flight mode (can also be called separation mode), where the ball-roller and cylindrical groove move freely, relative to each other across the clearance circle and no acting force between them. The other is the following mode (can also be called contact mode), where the two elements remain in contact, while the contact force is not zero.

Due to the discontinuities in the motion resulting from the clearance in the TBS joint, the complete motion of the crank–slider mechanism has to be described by two sets of equations. This will cause many difficulties in solving equations numerically.

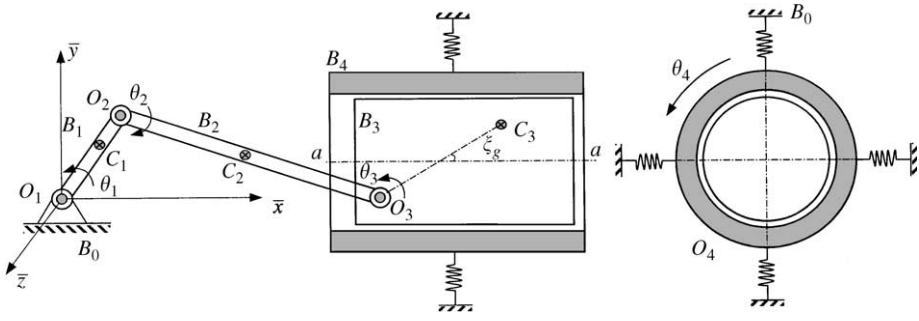


Figure 2. The crank–slider mechanism with clearance in the TBS joint.

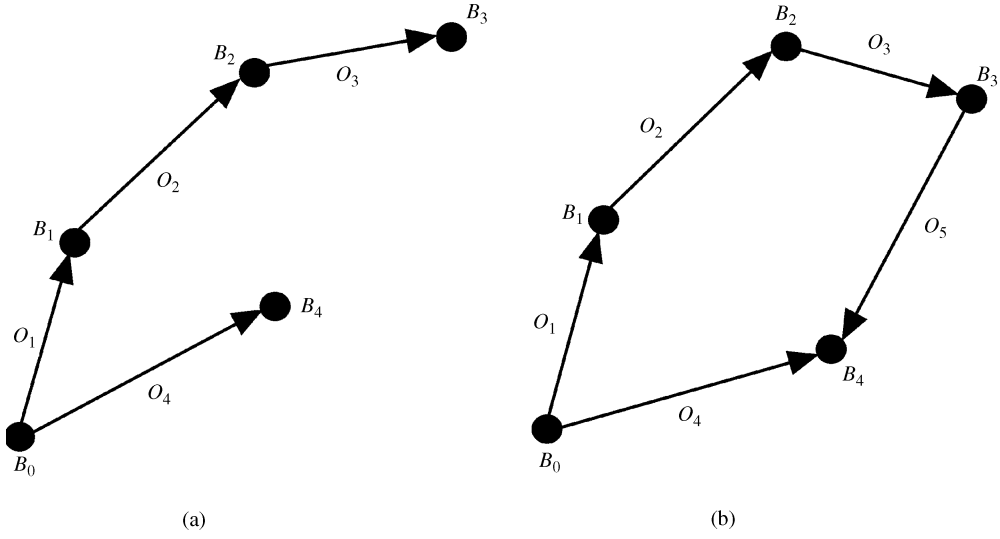


Figure 3. The topological structure of the mechanism with clearance in the TBS joint.

To make the two sets of equations as one set of consistent equations is an effective way to overcome the inadequacy. The consistent equations of motion can be obtained in the following. Topological map is used to illustrate different structures of the system in the two modes. Circle point denotes each rigid body $B_i$, straight line with arrow denotes each joint $O_i$. When the TBS joint is in free-flight mode, the system has invariable topological structure shown in Figure 3(a). It is defined as the basal system, in which there is no force exerted in the TBS joint. On the other hand, when the joint elements remain in contact, the system with topological structure shown in Figure 3(b) is called active system. Because of the elastic deformation of the element surface, the virtual work of the acting force between body $B_3$ and $B_4$ is no longer zero.

A complete contact model is assumed as a spring–dashpot system [10]. In the present work, an improved mathematical model of clearance joint was set up to approach the actual motion [11].

The law of elastic contact force $F_s$ versus displacement $\delta$ for the spring can be written as follows:

$$F_s = \frac{2}{3(k_1 + k_2)} \left(\frac{\pi m_a}{k(e)}\right)^{3/2} \left(\frac{1}{\Sigma\rho}\right)^{1/2} \delta^{3/2}, \tag{1}$$

$$k_i = 1 - \nu_i^2/E_i \quad (i = 1, 2). \tag{2}$$

Equation (1) can also be formulated as follows:

$$F_s = K\delta^{3/2}. \tag{3}$$

Since the energy loss is dependent on the approach velocity $\dot{\delta}$ and approach displacement between the two joint elements, the damping force can be modelled as

$$F_v = c\dot{\delta}, \tag{4}$$

where $c$ is a function of $\delta$ and can be calculated by the following formula:

$$c = f(\delta) = \mu\delta^n, \tag{5}$$

where $n$ is equal to unity for the analytical convenience.

Therefore, the contact force between the two joint elements can be obtained as follows:

$$p = \begin{cases} 0 & \text{(free-flight mode)}, \\ k\delta^{3/2} + \mu\delta\dot{\delta} & \text{(contact mode)}. \end{cases} \tag{6}$$

The basal system has four degrees of freedom, which is different from normal crank–slider mechanism, and its motion can be described by the following generalized co-ordinates:

$$q = [\theta_1, \theta_2, \theta_3, \theta_4]. \tag{7}$$

By using Kane method [12], the generalized velocity is written, in terms of the system degrees of freedom, as follows:

$$u_r = \dot{q}_j (r = j = 1, 2, 3, 4). \tag{8}$$

The kinematic parameters of each body $B_i$ can be expressed as

$$V_i = \sum_{r=1}^{N} v_i^{(r)} u_r + v_i^{(t)}, \qquad \omega_i = \sum_{r=1}^{N} \varpi_i^{(r)} u_r + \varpi_i^{(t)}, \tag{9, 10}$$

where $v_i^{(r)}$, $\varpi_i^{(r)}$ are the $r$th partial velocity or partial angular velocity of body $B_i$ and $v_i^{(t)}$, $\varpi_i^{(t)}$ are the terms independent of the generalized velocity. $v$, $\varpi$ can be written in matrix as shown in Appendix A.

According to the active or inertia force vector in Appendix A, the generalized active force $F^{(r)}$ and the generalized inertia force $F^{*(r)}$ can be obtained by

$$F^{(r)} = \sum_{i=1}^{4} (R_i v_i^{(r)} + L_i \varpi_i^{(r)}), \qquad F^{*(r)} = \sum_{i=1}^{4} (R_i^* v_i^{(r)} + L_i^* \varpi_i^{(r)}). \tag{11, 12}$$

Thus, the motion equations of the basal system can be derived as shown in equation (13), or in another form as equation (14).

$$\begin{aligned} &F^{(r)} + F^{*(r)} = 0 \\ &\dot{q}_r = u_r \end{aligned} \qquad (r = 1, 2, 3, 4), \tag{13}$$

$$M(\dot{u}_r, u_r, q_r, t) = 0. \tag{14}$$

Evidently, when any one group of ball-roller of the TBS joint makes contact with the groove, the basal system will change to the active one, and the above equations of motion

will not be applicable any more. Due to the contact force $p_i$ between the joint elements, a set of extra constraint equations were established as follows or written as equation (15) or (16), the details can be found in reference [11].

$$F_y = \sum_{i=1}^{3} \lambda_i (K\delta_i^{3/2} + \mu\delta_i\dot{\delta}_i)\sin\varphi_i,$$

$$M_{cz} = \sum_{i=1}^{3} \lambda_i (K\delta_i^{3/2} + \mu\delta_i\dot{\delta}_i)\sin\varphi_i[l_3\cos(\alpha + \xi_o) - R_d\sin\alpha\cos\gamma_i - \rho_3\cos(\alpha + \xi_g)], \quad (15)$$

$$M_{cx} = \sum_{i=1}^{3} \lambda_i[(K\delta_i^{3/2} + \mu\delta_i\dot{\delta}_i)\cos\varphi_i q_{iy} - (K\delta_i^{3/2} + \mu\delta_i\dot{\delta}_i)\sin\varphi_i q_{iz}],$$

$$\Phi(\dot{u}_r, u_r, q_r, t) = 0, \quad (16)$$

where $\lambda_i$ denotes the contact state of the group $i$ of ball-roller and groove

$$\lambda_i = \begin{cases} 1 & (r_i \geqslant r_0), \\ 0 & (r_i < r_0). \end{cases} \quad (17)$$

In fact, when the crank rotates continuously, contact mode of the TBS joint will be changing frequently and unpredictably. The basal system remains invariable unless the constraint equations take effect, and then the active one will be aroused. In order to distinguish whether the constraint equations is living or not, a special criterion $\lambda$ was defined as equation (18), which is determined by the kinetic parameters and external forces of joint elements.

$$\lambda = \sum_{i=1}^{3} \lambda_i. \quad (18)$$

From equations (14), (16) and (18), the consistent equations of motion of the crank–slider mechanism with clearance in the TBS joint can be completely described as

$$M(\dot{u}_r, u_r, q_r, t) + \lambda\Phi(\dot{u}_r, u_r, q_r, t) = 0, \quad (19)$$

where $q_r$ and $u_r$ have been defined in equations (7) and (8), $\dot{u}_r$ stands for one-order derivative of $u_r$, and $t$ stands for time.

The equations which are a set of coupled, non-linear one-order differential ones, having no analytical solution, need to be integrated numerically. In the process of the numerical simulation, the form of equation is consistent and the factor $\lambda$ is determined automatically. If $\lambda = 0$, then each group of ball-roller of the TBS joint is in free-flight mode, otherwise at least one group is in contact mode. In other words, the system varies from basal one to active one with the change of $\lambda$.

## 4. EXPERIMENTAL WORK

An experimental investigation corresponding to the theoretical analysis was carried out to discuss the dynamic performances of clearance in the TBS joint. A crank–slider mechanism mounted in the vertical plane was constructed (see Figure 4). The parameters of the chain are given in Appendix B. It was mounted on a heavy steel base. The input speed was provided by a speed-controlled DC motor, type Z400/40-220. The output shaft of the

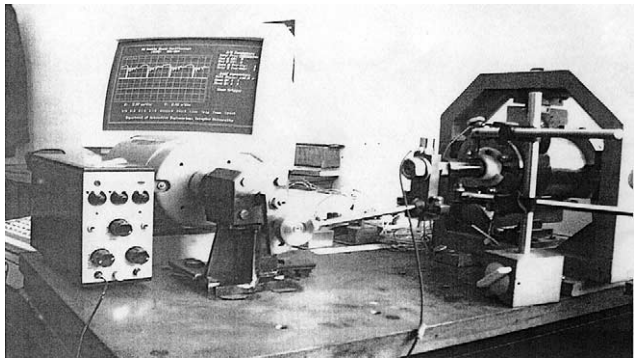

Figure 4. The crank–slider experimental rig.

motor was connected with the crank by a rigid coupling which had a large diameter so as to act like a flywheel to provide constant speed. Two sets of ball-rollers with different sizes were used to study the influence of the clearance size, while the driving speed can be easily changed over a large range by adjusting the motor voltage. The joints were very lightly oiled to minimize friction in the connections.

The speed of crank was monitored with an optical code speedometer. The additional motions $\alpha$ and $\beta$, displacements of the joint elements around $z$- and $x$-axis were measured by three eddy current transducers (sensitivity 8 mV/$\mu$m). One was for recording $\beta$ and the other two signals were combined to obtain the fluctuation of $\alpha$. The acceleration $\ddot{y}_3$ in the direction of $y$-axis of shaft 1 (see Figure 1) was monitored to indicate the impact caused by the joint clearance. A Brüel and Kjaer accelerometer, type 4366, and a charge amplifier, type 2635, sensitivity 44·6 Pc/g, were used here. The output cable of the charge amplifier was fixed on the shaft to minimize the electromagnetic disturbance. Because the drive torque $M_d$ of crank is equal to the output torque of the motor, it can be derived via the input power of motor and crank speed, considering the motor power factor at the same time. The input voltage and current of the motor were recorded. The signals were recorded simultaneously with the DP16 data acquisition system, which interfaced with a personal computer for storage and display of the results. The data can be processed further on computer. The results were obtained by the measurement repeated several times. Besides, some runs were first performed to get rid of the influence of the surface burr of the parts.

## 5. NUMERICAL AND EXPERIMENTAL RESULTS

The implicit variable-step Runge–Kutta method was employed to solve the motion equations (19); the initial time step was typically $10^{-5}$ s. The initial values were obtained from the nominal mechanism which had no clearance under the same conditions. However, the initial conditions were found to influence strongly the dynamic behavior of the mechanism during the first few cycles [9]. Extensive computer runs show that, if the simulation is allowed to continue over a large number of cycles, then a quasi-steady state may happen. Therefore, the numerical and experimental results for comparison will be obtained in quasi-steady state.

No numerical problems were encountered as the program switched from one mode to another mode, by virtue of two reasons, one is the small time step, and the other is using a non-linear spring–dashpot model while impact happens which improves the stability of the mode-change effectively.

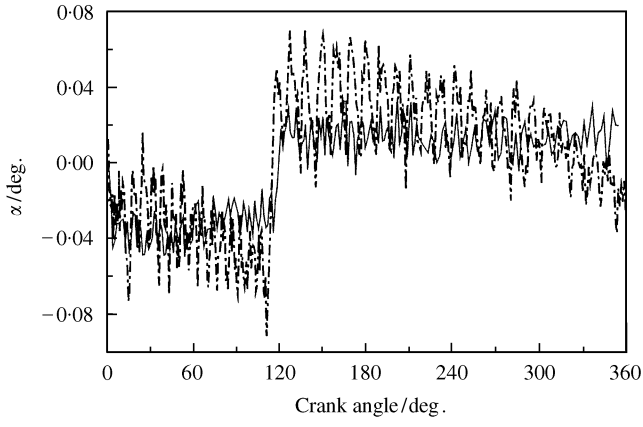


Figure 5. The additional displacement $\alpha$: –·–·–, experiment; ——, theory.

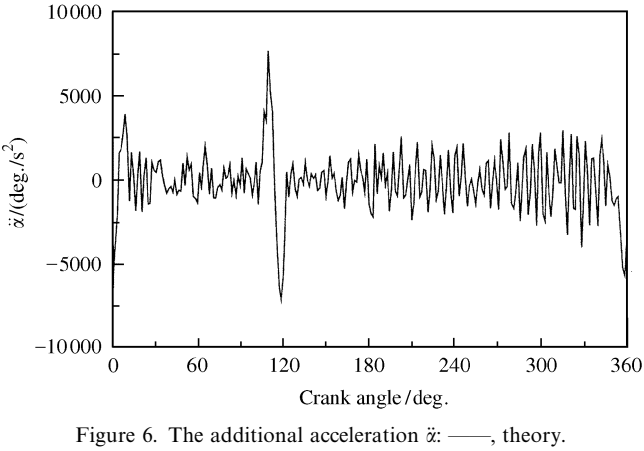


Figure 6. The additional acceleration $\ddot{\alpha}$: ——, theory.

The equations were integrated numerically over the range of the input crank speed $\omega = 60$–$1500$ r.p.m., the clearance size $r_0 = 0{\cdot}06$–$1{\cdot}5$ mm, the stiffness of contact surface $K = 10 \times 10^8$ N/m and the coefficient of viscous damping $\mu = 2$ N s/m. The experimental data were only recorded at speeds in the range 75–429 r.p.m., with clearances 0·07 and 0·13 mm in the TBS joint.

The effects of the clearance on the dynamic characteristics were studied comprehensively, including the additional motion of the mechanism, the acceleration of joint element, the joint force, the contact mode and the input torque. These will be discussed in detail as follows according to the numerical and experimental results.

### 5.1. ADDITIONAL MOTION

Figures 5 and 6 show the angular displacement $\alpha$ and acceleration $\ddot{\alpha}$ of body $B_3$ around $z$-axis. Figures 7 and 8 show the translational displacement $y_3$ and acceleration $\ddot{y}_3$ of body $B_3$ in the direction of $y$-axis. The numerical results (solid line) were compared with the experimental ones (dash–dot line). These additional displacements and accelerations become zero when clearance is zero. (The angular displacement $\beta$ and acceleration $\ddot{\beta}$ of body $B_4$ around $x$-axis have the same change laws.)

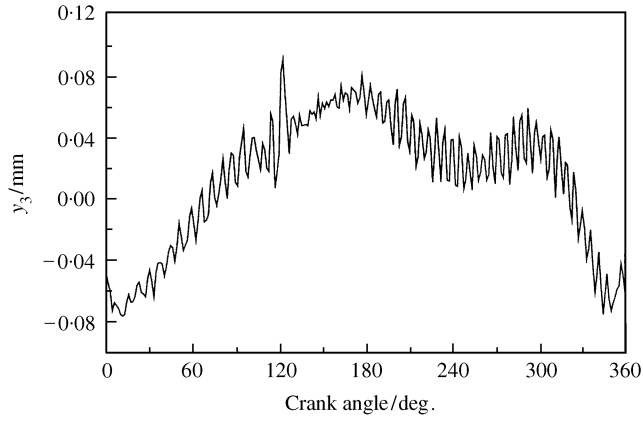


Figure 7. The translational displacement $y_3$: ——, theory.

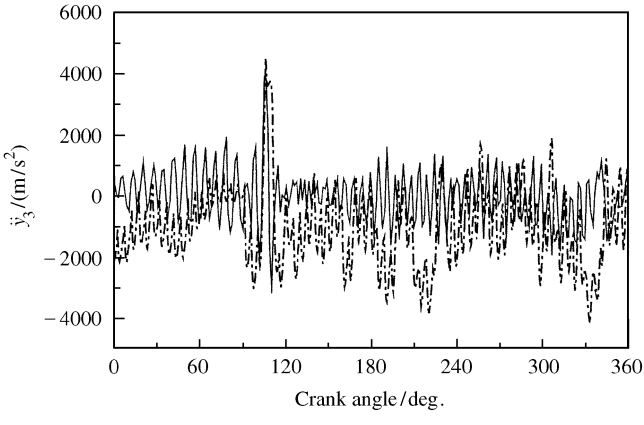


Figure 8. The translational acceleration $\ddot{y}_3$: –·–·–, experiment; ——, theory.

It can be seen from these figures that

(1) The clearance effect cannot be ignored, especially for the changes in the values of accelerations as compared with the case without clearance.
(2) These dynamic parameters change suddenly at a special crank angle (about 113° here). The occurrence is owing to the change of direction of the torque exerted on body $B_3$ around $z$-axis at this angle. The results from simulation show that the angle depends on the structural parameters of the mechanism (the lengths of linkages), and almost has nothing to do with the size of clearance.
(3) The theoretical response shows good agreement with the experimental response to some extent.

## 5.2. INPUT TORQUE

Figure 9 displays the variation of the input torque over one full cycle of the crank rotation. We can make the following remarks regarding this figure:

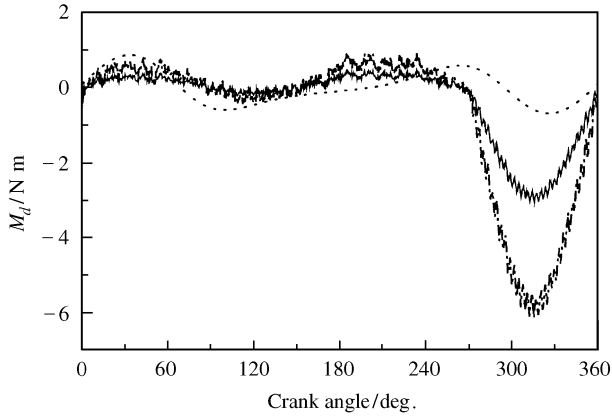


Figure 9. The variation of the input torque $M_d$: –·–·–, experiment; ——, theory with clearance; - - -, theory without clearance.

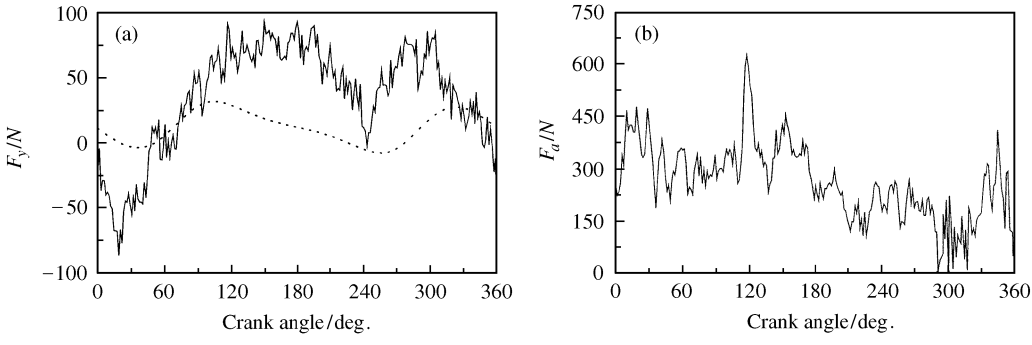


Figure 10. (a) The constraint force $F_y$: - - -, theory with clearance; ——, theory without clearance; (b) The contact force $F_a$: ——, theory.

(1) There is some small variation of the input torque, which has the same trend of magnitude, period as the variation of the dynamic behavior in section 5.1.
(2) The curves with or without clearance (dotted line) have the same trend, that is, same waveform. Comparing the minima, maxima, and crossing points, we can find that the phase of the torque when clearances exist generally leads to that without it. This is expected since the presence of clearance induces effects similar to that of the "dead-time" in feedback loops, which in turn are associated with positive phase shifts.
(3) The theoretical trace of torque matches the experimental one except for some phase shift.

### 5.3. JOINT FORCE

Analysis of the constraint forces acting at such a joint with or without clearance in the mechanism is required for the calculation of strength and wear of the system. Figure 10(a) shows the constraint force $F_y$ of the TBS joint along $y$-axis, and Figure 10(b) shows the contact force $F_a$ between one group of ball-roller and groove, which is normal to the plane of contact. Figure 11 shows the joint constraint force $F_{1y}$ of joint $O_2$ between crank and link along $y$-axis.

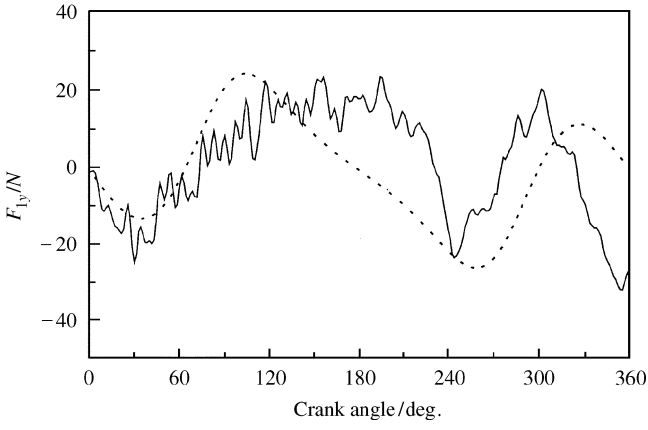


Figure 11. The joint constraint force $F_{1y}$ of joint $O_2$: ——, theory with clearance; - - -, theory without clearance.

The following remarks can be drawn from the analysis of the three figures:

(1) There is a remarkable variation of the contact force because the joint elements move relatively to each other and elastic deformation occurs on the contact surface undesirably. At the same special value of crank angle 113°, a sudden shock of contact force occurs, just as the change of dynamic parameters of joint elements does (stated in section 5.1).
(2) When the contact force equals zero, this group of ball-roller and groove separates from each other; otherwise they remain in contact. Since the contact force can never be in tension, it can be regarded as a token to identify whether the clearance joint is in free-flight mode or the following mode.
(3) The force $F_{1y}$ of joint $O_2$ is similar to that of nominal mechanism, except for some high-frequency, low-amplitude oscillation, and it has no sudden shock at the crank angle 113°. It is because the geometric structure of the TBS joint improves the distribution of forces of the system, and impacts caused by clearance are reduced.
(4) The resultant force $F_y$ of the three contact forces has the same peculiarity as $F_{1y}$. In contrast to the normal prismatic joint in reference [2], the TBS joint has an advantage to improve the dynamic behavior of the mechanism.

Besides, Figure 12 illustrates the distribution of the three contact forces with the polar co-ordinates. Circumferential values represent the direction of the contact force relative to $z$-axis, and radial distances denote their amplitude. It is observable that the three contact forces, respectively, distribute in a certain limited region. It can be concluded that wear value must be much higher in these special regions of the TBS joint. Thus, some extra surface treatment should be carried out to enhance its abrasion resistance and prolong the life of the joint.

### 5.4. CONTACT STATE

Due to the clearance in the TBS joint, the elements stay in free-flight mode or contact mode. Figure 13 shows the contact state of each group of joint elements in one cycle of crank rotation. The hatched regions indicate the separate mode (with frequent impact) and the rest is contact state. It can be found that there are at least two groups in contact at any

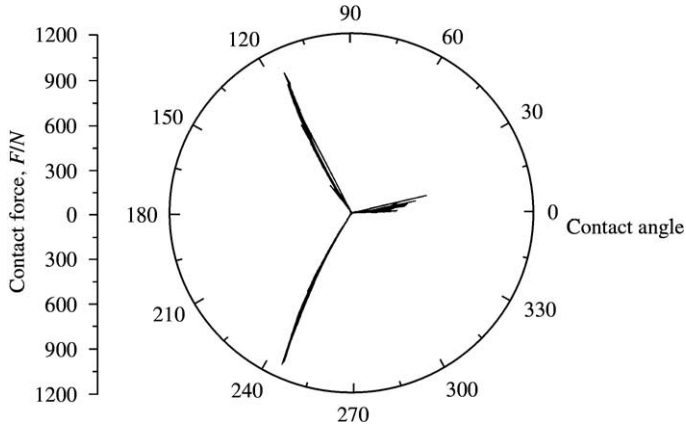


Figure 12. The distribution of the contact forces.

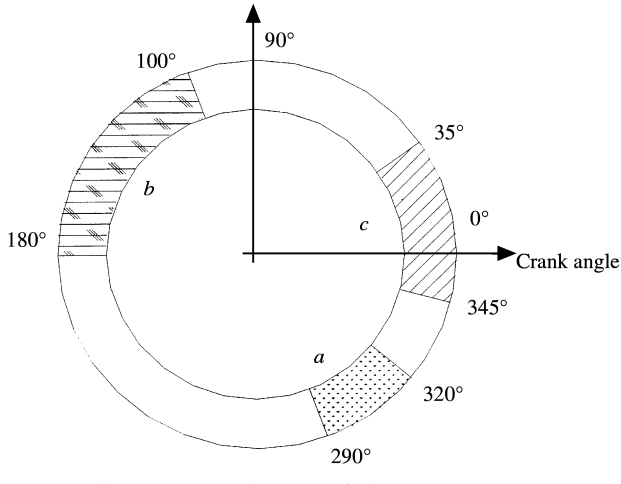


Figure 13. The contact state in one cycle ($r_0 = 0{\cdot}07$ mm, $\omega = 75$ r.p.m.).

angle of crank rotation, and the complete breakaway between body $B_3$ and $B_4$ never occurs. As a result, no large impact takes place. This agrees with the result in section 5.3. (In the above Figures 5–13, $r_0 = 0{\cdot}07$ mm, $\omega = 75$ r.p.m.).

## 5.5. THE MAIN INFLUENCING FACTORS

Figure 14 shows the experimental results of the additional displacement $\alpha$ and the driving torque $M_d$ at different clearance sizes $r_0$ (data in Figure 14 were smoothed with a low-pass filter with a bandwidth of 40 Hz), and Figure 15 displays the variation of $\delta_\alpha$ and $\eta_{Md}$ at different speeds which are defined by the following equations:

$$\delta_\alpha = \alpha_{max} - \alpha_{min}, \qquad \eta_{Md} = |\max(M_d - M_{d0})|. \tag{20, 21}$$

The effect of increasing clearance size is (1) to make a moderate growth of the driving torque, and (2) not only to increase the amplitude of the additional displacements, but also to intensify the impact at the sudden change angle.

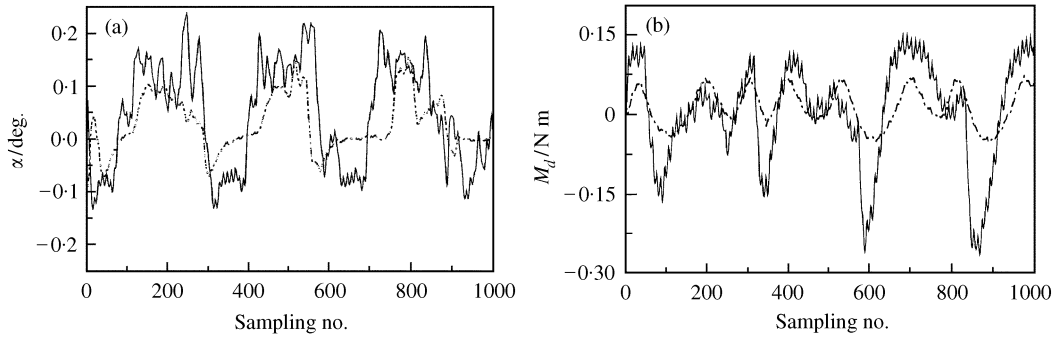


Figure 14. Effects of clearance size ($\omega = 183$ r.p.m.): ——, $r_0 = 0{\cdot}13$ mm; –·–·–, $r_0 = 0{\cdot}07$ mm.

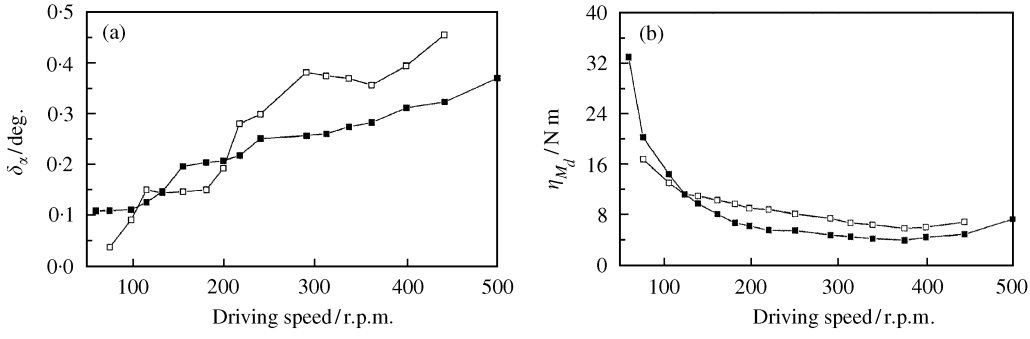


Figure 15. The variation of $\delta_\alpha$ and $\eta_{Md}$ at different speeds ($r_0 = 0{\cdot}13$ mm): —■—, theory; —□—, experiment.

$\delta_\alpha$ drops gradually with the growth of driving speed, while $\eta_{Md}$ is not a simple monotonous function of driving speed. According to the numerical results, we can observe that at a low driving speed, $\eta_{Md}$ drops steeply with speed, then levels off for a short range, and when driving speed is more than 380 r.p.m., $\eta_{Md}$ increases moderately with speed. According to the experimental record, the shift value is about 400 r.p.m., slightly bigger than the theoretical one. This is because of inertia moment. At low speed, the gravitational forces can be seen to dominate the motion of the mechanism, but inertia moment becomes more important as speed increases further.

## 6. CONCLUSIONS AND PROSPECTS

(1) The mathematical model of the new-type tripod-ball sliding joint with clearance established in this paper is effective to study its dynamic effects on the behavior of the crank–slider mechanism. The results verify that the TBS joint has the advantage to weaken the impact caused by clearance.

(2) The consistent equations for both free-flight and following mode are presented by defining a mode-change criterion. The method may be extended for mechanisms with multiple clearance joints or other complicated systems, and thus, has universal significance.

(3) The influence of the joint clearance is investigated, and some significative results are obtained.

Other factors such as the stiffness and the coefficient of viscous damping of contact surface have an influence on the dynamics of the mechanism, which have also been studied quantitatively. The results are of great significance to the further study of the dynamics of the mechanical system with clearance.

## ACKNOWLEDGMENTS

The authors would like to acknowledge the Tsinghua University Foundation for the support of this research under Grant no. 0139518(S9502).

## REFERENCES

1. C. W. STAMMERS and M. GHAZAVI 1991 *Journal of Sound and Vibration* **150**, 301–315. A theoretical and experimental study of the dynamics of a four-bar chain with bearing clearance: pin motion, contact loss and impact.
2. ZHANG ZHAODONG 1992 *Ph.D. Dissertation*, *Tsinghua University*. Dynamic analysis and synthesis of link mechanisms with elastic links and clearances in joints.
3. F. FARAHANCHI and S. W. SHAW 1994 *Journal of Sound and Vibration* **177**, 307–324. Chaotic and periodic dynamics of a slider–crank mechanism with slider clearance.
4. H. S. TZOU and Y. RONG 1991 *American Institute of Aeronautics and Astronautics Journal* **29**, 81–88. Contact dynamics of a spherical joint and a jointed truss-cell system.
5. T. KAKIZAKI, J. F. DECK and S. DUBOWSKY 1993 *American Society of Mechanical Engineers Journal of Mechanics and Design* **115**, 839–847. Modeling the spatial dynamics of robotic manipulators with flexible links and joint clearances.
6. L. D. SENVIRATNE and S. W. E. EARLES 1996 *Proceedings of the Institution of Mechanical Engineers. Part C*: *Journal of Mechanical Engineering Science* **210**, 215–223. Analysis of a four-bar mechanism with a radially compliant clearance joint.
7. R. JUNGKEUN and A. ADNAN 1996 *Mechanism & Machine Theory* **31**, 121–134. Dynamic response of a revolute joint with clearance.
8. B. MIEDEMA and W. M. MANSOUR 1976 *American Society of Mechanical Engineers Journal of Engineering for Industry* **11**, 1319–1323. Mechanical joints with clearance: a three-mode model.
9. L. D. SENVIRATNE and S. W. E. EARLES 1992 *Mechanism & Machine Theory* **27**, 307–321. Chaotic behavior exhibited during contact loss in a clearance joint of a four-bar mechanism.
10. S. DUBOWSKY and F. FREUDENSTEIN 1971 *American Society of Mechanical Engineers Journal of Engineering for Industry* **93B**, 305–309. Dynamic analysis of mechanical systems with clearance. part 1. formation of dynamic model.
11. JIA XIAOHONG 1999 *Ph.D. Dissertation*, *Tsinghua University*. Investigation on the dynamics of the universal transmission system of high-speed locomotive and tripod-ball sliding joint with clearance.
12. J. WITTENBURG 1977 *Dynamics of Systems of Rigid Bodies*. Stuttgart: Teubner.

## APPENDIX A: SOME TERMS IN MOTION EQUATIONS

$v =$

$$\begin{bmatrix} -\rho_1(\sin q_1\bar{x}_0 - \cos q_1\bar{y}_0) & -l_1(\sin q_1\bar{x}_0 - \cos q_1\bar{y}_0) & -l_1(\sin q_1\bar{x}_0 - \cos q_1\bar{y}_0) & 0 \\ 0 & -\rho_2(\sin q_2\bar{x}_0 + \cos q_2\bar{y}_0) & -l_2(\sin q_2\bar{x}_0 + \cos q_2\bar{y}_0) & 0 \\ 0 & 0 & -\rho_3(\sin q_3\bar{x}_0 - \cos q_3\bar{y}_0) & 0 \\ 0 & 0 & 0 & 0 \end{bmatrix},$$

$$\varpi = \begin{bmatrix} \bar{z}_0 & 0 & 0 & 0 \\ 0 & -\bar{z}_0 & 0 & 0 \\ 0 & 0 & \bar{z}_0 & 0 \\ 0 & 0 & 0 & \bar{x}_0 \end{bmatrix},$$

$$R = [-m_1 g\bar{y}_0 - m_2 g\bar{y}_0 - m_3 g\bar{y}_0 \;\; 0]^{\mathrm{T}}, \qquad L = [M_d\bar{z}_0 \;\; 0 \;\; 0 \;\; M_f]^{\mathrm{T}},$$

$$R^* = \begin{bmatrix} m_1[\rho_1(\dot{u}_1 \sin q_1 + u_1^2 \cos q_1)\bar{x}_0 - \rho_1(\dot{u}_1 \cos q_1 - u_1^2 \sin q_1)\bar{y}_0] \\ m_2[(l_1\dot{u}_1 \sin q_1 + l_1u_1^2 \cos q_1 + \rho_2\dot{u}_2 \sin q_2 + \rho_2u_2^2 \cos q_2)\bar{x}_0 \\ -(l_1\dot{u}_1 \cos q_1 - l_1u_1^2 \sin q_1 - \rho_2\dot{u}_2 \cos q_2 + \rho_2u_2^2 \sin q_2)\bar{y}_0] \\ m_3[(l_1\dot{u}_1 \sin q_1 + l_1u_1^2 \cos q_1 + l_2\dot{u}_2 \sin q_2 + l_2u_2^2 \cos q_2 + \\ \rho_3\dot{u}_3 \sin(q_3 + \xi_g) + \rho_3u_3^2 \cos(q_3 + \xi_g))\bar{x}_0 - \\ (l_1\dot{u}_1 \cos q_1 - l_1u_1^2 \sin q_1 - l_2\dot{u}_2 \cos q_2 + l_2u_2^2 \sin q_2 \\ + \rho_3\dot{u}_3 \cos(q_3 + \xi_g) - \rho_3u_3^2 \sin(q_3 + \xi_g))\bar{y}_0] \\ 0 \end{bmatrix},$$

$$L^* = [-J_1\dot{u}_1\bar{z}_0 \;\; J_2\dot{u}_2\bar{z}_0 \;\; -J_3\dot{u}_3\bar{z}_0 \;\; -J_4\dot{u}_4\bar{x}_0]^{\mathrm{T}}.$$

## APPENDIX B: DATA FOR THE MECHANISM (see Table B1)

TABLE B1

| Body $B_i$ | $m_i$ (kg) | $l_i$ (m) | $\rho_i$ (m) | $J_i$ (kg m$^2$) |
|---|---|---|---|---|
| Crank | 0·2 | 0·03 | 0·017 | $1{\cdot}43 \times 10^{-4}$ |
| Link | 0·2 | 0·15 | 0·046 | $6{\cdot}6 \times 10^{-4}$ |
| Slider | 1·05 | — | 0·105 | $5{\cdot}07 \times 10^{-3}$ |
| Groove | 5·02 | — | — | $6{\cdot}69 \times 10^{-3}$ |

## APPENDIX C: NOMENCLATURE

| | |
|---|---|
| $E_i$ | Young's modulus ($i = 1, 2$) |
| $F_a$ | contact force |
| $F_{1y}$ | $y$-component of force of joint $O_2$ |
| $F_s$ | the elastic contact force |
| $F_v$ | the damping force |
| $F^{*(r)}$ | generalized inertia force |
| $F^{(r)}$ | generalized active force |
| $g$ | gravitational constant |
| $J_i$ | moment of inertia of body $B_i$ ($i = 1, 2, 3, 4$) |
| $K$ | the equivalent stiffness of the spring |
| $k(e)$, $m_a$, $\Sigma\rho$ | some parameters obtained from the geometry for the contacting joint elements |
| $L$, $L^*$ | active and inertia moment |
| $l_i$ | length of body $B_i$ ($i = 1, 2$) |

| | |
|---|---|
| $m_i$ | mass of body $B_i$ ($i = 1, 2, 3, 4$) |
| $M_{d0}$ | the input torque of nominal mechanism |
| $M_d$ | input torque |
| $q$ | generalized co-ordinate |
| $r_0$ | the clearance size |
| $r_i$ | the actual displacement between each center point of group $i$ of ball-roller and groove ($i = 1, 2, 3$) |
| $R_d$ | the distance between the center of ball-roller and center of tripod base (in Figure 1) |
| $R$, $R^*$ | active and inertia force |
| $u$ | generalized velocity |
| $V_i$ | velocity of mass center $C_i$ of body $B_i$ ($i = 1, 2, 3, 4$) |
| $(\bar{x}_0, \bar{y}_0, \bar{z}_0)$ | unit vector of the absolute rectangular co-ordinates |
| $y_3$, $\ddot{y}_3$ | translational displacement and acceleration of body $B_3$ in the direction of $y$-axis |
| $\alpha$, $\ddot{\alpha}$ | angular displacement and acceleration of body $B_3$ about $z$-axis |
| $\beta$, $\ddot{\beta}$ | angular displacement and acceleration of body $B_4$ about $x$-axis |
| $\lambda$ | mode-change criterion |
| $\delta$ ($\delta_i$) | the deflection of the contact surface (of group $i$, $i = 1, 2, 3$) |
| $\dot{\delta}$ ($\dot{\delta}_i$) | one-order derivative of the deflection of the contact surface (of group $i$, $i = 1, 2, 3$) |
| $\gamma_i$ | a value equal to $120^\circ(i - 1)$ ($i = 1, 2, 3$) |
| $\xi_g$ | the angle between the axis of tripod base 'a–a' and the line across $O_3$ and $C_3$ (in Figure 2) |
| $\rho_i$ | center of mass of body $B_i$ from joint $O_i$ ($i = 1, 2, 3$) |
| $\theta$ | rotational angle of body $B_i$ ($i = 1, 2, 3, 4$) |
| $\varphi$ | contact angle |
| $\mu$ | a material property, independent of surface deformation |
| $v_i$ | the Poisson ratio for each joint element ($i = 1, 2$) |
| $v$ | partial velocity |
| $\omega$ | the crank speed |
| $\omega_i$ | angular velocity of body $B_i$ ($i = 1, 2, 3, 4$) |
| $\varpi$ | partial angular velocity |